

COMPUTATIONAL STUDY OF PARTICLE/LIQUID FLOWS IN CURVED/COILED MEMBRANE SYSTEMS

Prashant Tiwari¹, Steven P. Antal^{1,2}, Michael Z. Podowski^{1,2}*

¹*Department of Mechanical, Aerospace and Nuclear Engineering,*

²*Center for Multiphase Research,*

Rensselaer Polytechnic Institute,

Troy, NY 12180, USA

() Tel: 518-276-4000, Fax: 518-276-3055*

Email: podowm@rpi.edu

Key words: Membrane filtration; Dean vortices, Particle/liquid system; Multi-field model; CFD

Prepared for presentation at the 2004 Annual Meeting, Austin, TX, Nov. 7-12

Copyright © Prashant Tiwari, Steven P. Antal, Michael Z. Podowski, Rensselaer Polytechnic Institute, Troy, NY.

AIChE shall not be responsible for statements or opinions contained in papers or printed in its publications.

Abstract

When a fluid flows inside a curved tube, the centrifugal forces due to the curvature are balanced by the pressure gradient across the tube. These centrifugal forces induce secondary flows, known as Dean vortices, that have proven to be very useful in many engineering applications.

Recently, the use of Dean vortices in membrane filtration has become one of the most effective methods for reducing the concentration polarization. Various configurations of modules have been developed for this purpose; it has also been confirmed experimentally that using curved, rather than straight, membrane tube geometries allows for increasing the mass flux and leads to improved membrane efficiency. Until now, both theoretical and computational works on the effect of curvature on membrane system performance have been limited to simplified (1D or 2D), mainly single-phase, flow models inside the membrane tubes. Since the actual industrial filtration operations involve particle/liquid slurries, it is important to understand the effect of geometry and flow conditions on particle distribution in curved-geometry tubes and channels.

The objective of this paper is to present the results of theoretical and numerical analyses of dilute liquid/particle two-phase flows in straight tube and U-bend membrane systems that are used for micro- and nano-filtrations. The numerical analysis is based on CFD simulations performed using a state of the art two-phase flow model and a next-generation multi-phase flow computer code, NPHASE. The main part of this paper is concerned with rigorous modeling of shear-induced diffusion force due to liquid cross-flow. The effect of liquid flow across membrane surface on particle distribution is also studied in detail.

1. Introduction

Cross-flow filtration is one of the most popular modes of industrial operations. Several industrial fluids comprise of particle-liquid suspensions, so it is important to separate the solute, which is mostly particulate matter, from the solution. Though cross-flow filtration is a widely used mode, this process has not been well studied in terms of particle/liquid fluid mechanics. Needless to say, detailed two-phase particle-liquid studies are important in order to understand the cross-flow filtration behavior.

In cross-flow filtration, as compared to the flow inside a solid tube, particle trajectories can be affected by the suction through the wall. For dilute concentrated solutions, the back-transport mechanisms (inertial lift, Brownian diffusion, shear-induced diffusion, etc.) could play a significant role in moving particles away from the wall. Due to the shear from the tangential flowing liquid, the cake layer does not grow indefinitely, as some particulate matter gets swept by the suspension towards the filter exit. This phenomenon is known as *shear-induced diffusion*.

For smaller particles, Brownian diffusion and shear-induced diffusion are the most dominant back-transport mechanisms. It was shown before (for, example, see Belfort et. al. [1]) that for micro-particles (the diameters of which are of the order of a few microns), the permeate flux

attained by particles due to shear-induced diffusion is much higher than Brownian diffusion. Hence, one can consider only the shear-induced diffusion to determine the particle concentration profile for such particles, without causing a significant error.

In this paper, a novel way is presented to mechanistically model the shear-induced diffusion force that affects the near-wall particle concentration profile in permeable membrane modules, and to account for this force in full 3-D simulations of particulate flow in curved membrane tubes.

2. Multidimensional CFD Model of Liquid/Particle Flows

The present analysis uses a multidimensional model of dilute flows of particles dispersed in a continuous liquid field. The governing mass and momentum conservation equations (the energy equation has a negligible effect on the flow and can be ignored) for each, the continuous liquid and the dispersed particles, are determined with respect to a common physical and computational domain, and are given by [2,3]

Mass Conservation

Continuous liquid

$$\frac{\partial(\alpha_l \rho_l)}{\partial t} + \nabla \cdot (\alpha_l \rho_l \mathbf{v}_l) = 0 \quad (1)$$

Dispersed particles

$$\frac{\partial(\alpha_p \rho_p)}{\partial t} + \nabla \cdot (\alpha_p \rho_p \mathbf{v}_p) = 0 \quad (2)$$

Momentum Conservation

Continuous liquid

$$\begin{aligned} \frac{\partial}{\partial t}(\alpha_l \rho_l \mathbf{v}_l) + \nabla \cdot (\alpha_l \rho_l \mathbf{v}_l \mathbf{v}_l) = & -\alpha_l \nabla p_l - (p_l - p_{li})(\nabla \alpha_l) \\ & + \left(\underline{\underline{\tau_l}} - \underline{\underline{\tau_{li}}} \right) \cdot \nabla \alpha_l + \alpha_l \left(\nabla \cdot \underline{\underline{\tau_l}} \right) + \alpha_l \rho_l \mathbf{g} + \mathbf{M}_l^D + \mathbf{M}_l^{ND} \end{aligned} \quad (3)$$

Dispersed particles

$$\begin{aligned} \frac{\partial}{\partial t}(\alpha_p \rho_p \mathbf{v}_p) + \nabla \cdot (\alpha_p \rho_p \mathbf{v}_p \mathbf{v}_p) = & \\ - \alpha_p \nabla p_l + \alpha_p \nabla \cdot \underline{\underline{\tau_{li}}} + \alpha_p \rho_p \mathbf{g} - \mathbf{M}_l^D - \mathbf{M}_l^{ND} - \alpha_p \nabla (p_{li} - p_l) \end{aligned} \quad (4)$$

where α_p is the local volumetric concentration of particles, M_l^D and M_l^{ND} are the interfacial drag and non-drag forces, respectively, per unit volume of the fluid. In the present study we have incorporated the effect of shear-induced diffusion force as a non-drag force.

3. Mechanistic Model of Shear-Induced Diffusion Force

In order to properly incorporate the effect of shear-induced diffusion in the two-phase particle/liquid momentum balance equation, this phenomenon should be considered in terms of an interfacial force. In this section, a novel approach is presented to model the shear-induced diffusion effect as a non-drag force which can be used in the phasic momentum conservation equation.

3.1 Diffusion-Induced Particle Velocity

In cross-flow membrane systems, solvent flows out of the membrane in the tangential direction. Particles move towards the wall with the outgoing liquid, but cannot penetrate the porous membrane wall (have a 100% retention). This, in turn, results in an increased particle concentration at the wall. The backtransport mechanism pushes the solute (particles) to the bulk flow (see Figure. 1).

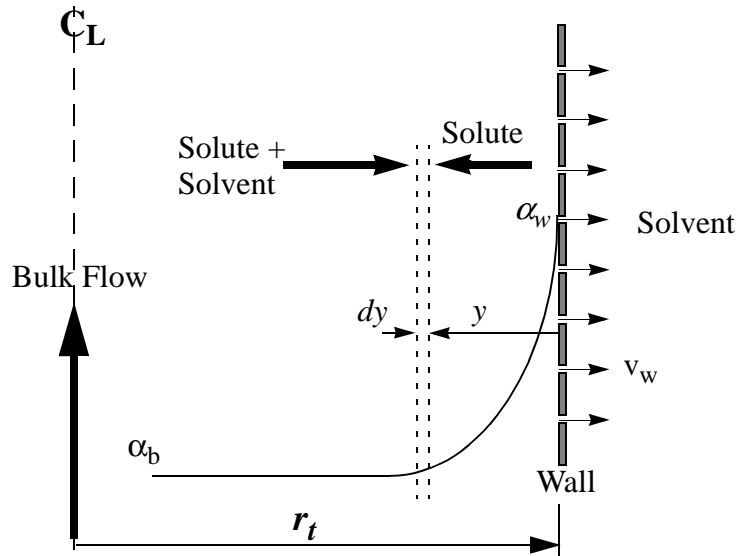


FIGURE 1. Schematic representation of membrane transport

The mass flux of particles moving away from the wall can be expressed as [4]:

$$\alpha_p \rho_p v_p = -\rho_p D \frac{d\alpha}{dy} \quad (5)$$

where ρ_p is the particle density, v_p is the particle velocity away from the wall, α_p is the particle volume fraction, and D [m²/s] is the total diffusion coefficient which accounts for the combined effects of various diffusion phenomena (Brownian diffusion, shear-induced diffusion, etc.).

In general, a diffusion coefficient, D , can be written in the form

$$D = D_0(kT, \tau_w, D_p, \mu_0, \dots)D(\alpha_p) \quad (6)$$

where D_0 is the particle-volume-fraction-independent part, and $D(\alpha_p)$ is a dimensionless diffusion multiplier which depends only on particle volume fraction, α_p .

Eq.(5) can be rewritten as

$$j_p = \alpha_p v_p = -D \frac{d\alpha_p}{dy} \quad (7)$$

where j_p is the superficial velocity of the particles back-transported to the bulk liquid.

From Eq.(7), it is clear that diffusion-induced particle velocity can be represented as

$$v_p = -\frac{D}{\alpha_p} \frac{d\alpha_p}{dy} = -D \frac{d}{dy} [\ln(\alpha_p)] \quad (8)$$

The direction of the velocity, v_p , is always away from the wall or towards the decreasing concentration gradient; hence, this velocity has a negative sign.

3.2 Force Due to Shear-Induced Diffusion

In order to include the backtransport mechanism in the phasic momentum conservation equation, this phenomenon must be represented in terms of a force. The concept of mobility [5] can be used for this purpose.

Mobility is defined as the velocity attained by particles when a unit driving force is applied on them. Thus, we write

$$\mathbf{F}_p = \frac{\mathbf{v}_p}{\lambda} = \mathbf{v}_p \Omega \quad (9)$$

where \mathbf{F}_p is the force acting on particles, \mathbf{v}_p is the average velocity attained by particles (m/s), and $\lambda = \Omega^{-1}$ (s/kg) is the lumped particle mobility.

In general, particle mobility can be attained by various back-transport mechanisms, such as Brownian diffusion, shear-induced diffusion, etc. The total mobility can be defined as the sum of mobility components attained by the various mechanisms

$$\lambda = \lambda_B + \lambda_{SI} + \lambda_{other} \quad (10)$$

or

$$\frac{1}{\lambda} = \Omega = \left(\frac{1}{\Omega_B} + \frac{1}{\Omega_{SI}} + \frac{1}{\Omega_{other}} \right)^{-1} \quad (11)$$

where $\lambda_B = \Omega_B^{-1}$, is the mobility attained due to Brownian diffusion and $\lambda_{SI} = \Omega_{SI}^{-1}$, is the mobility attained due to shear-induced diffusion.

As mentioned earlier, for small micro-particles, the effect of shear induced diffusion is much higher than that of the Brownian diffusion. Hence, in the following sections we take account of the shear induced diffusion only.

The inverse of particle mobility due to shear-induced diffusion can be described as

$$\Omega_{SI} = \frac{1}{\lambda_{SI}} = C_{SI} \frac{|\underline{\tau}| V_p}{D_{SI}} \quad (12)$$

where D_{SI} is the shear-induced diffusion coefficient, $|\underline{\tau}|$ is the magnitude of local shear stress, and V_p is the volume of particle.

Now, using Eq.(9), the force due to shear-induced diffusion becomes

$$F_{SI} = \frac{v_{p,SI}}{\lambda_{SI}} = C_{SI} v_{p,SI} \frac{|\underline{\tau}| V_p}{D_{SI}} \quad (13)$$

where $v_{p,SI}$ is the average velocity attained by a particle as a result of the shear induced diffusion force.

The term, C_{SI} , in Eqs.(12) and (13) is the shear-induced dispersion coefficient. As it is shown later in this section, C_{SI} can be uniquely determined as function of the particle volume fraction, α_p .

A summary of the existing models for the shear-induced diffusion coefficient is given in Table 1.

TABLE 1. Shear-induced diffusion coefficients

Equation	$D_{0, SI}$	D_{SI}	Ref.
$D_{SI} = 0.03 \frac{\tau_w D_p^2}{\mu}$	$\frac{\tau_w D_p^2}{\mu}$	0.03	Eckstein et al. [6]
$D_{SI} = 0.33 \frac{\tau_w D_p^2 \alpha_p^2}{\mu} (1 + 0.5 e^{8.8 \alpha_p})$	$\frac{\tau_w D_p^2}{\mu}$	$0.33 \alpha_p^2 (1 + 0.5 e^{8.8 \alpha_p})$	Leighton & Acrivos [7]

It is important to note that Eq.(13) determines the force is acting on a single particle. In order to represent the average force acting on all particles per unit volume, M_{SI} , we multiply Eq.(13) by particle number density, n'''

$$M_{SI} = \frac{v_{p, SI}}{\lambda_{SI}} n''' = C_{SI} V_{p, SI} \left| \frac{\tau}{\dot{\gamma}} \right| \frac{V_p}{D_{SI}} n''' \quad (14)$$

Interestingly, the product, $V_p n'''$, is the total volume occupied by particles per unit volume of the mixture, which is the definition of particle volume fraction

$$\alpha_p = V_p n''' \quad (15)$$

Now, Eq.(14) can be further simplified by utilizing the particle velocity definition given by Eq.(8). Thus, we write

$$M_{SI} = C_{SI} \left(-\frac{D_{SI} d\alpha_p}{\alpha_p dy} \right) \left| \frac{\tau}{\dot{\gamma}} \right| \frac{\alpha_p}{D_{SI}} \quad (16)$$

E.(16) can be simplified to the following form

$$M_{SI} = -C_{SI} \left| \frac{\tau}{\dot{\gamma}} \right| \frac{d\alpha_p}{dy} \quad (17)$$

Eq.(17), can be described as the force per unit volume acting on the particles as a result of shear-induced diffusion. This force acts away from the wall and towards the decreasing concentration gradient; hence, it is represented by a negative sign. It is interesting to note that the final form of the shear-induced diffusion force is proportional to the magnitude of shear

stress, $\left| \frac{\tau}{\dot{\gamma}} \right|$, and to the particle concentration gradient, $\frac{d\alpha_p}{dy}$.

By taking advantage of Davis & Leighton [8] results, the shear-induced dispersion coefficient we can determined as a function of particle volume fraction

$$C_{SI} = 5.94\alpha_p^2(1 + 0.5e^{8.8\alpha_p}) \quad (18)$$

4. Results and Discussion

4.1 Three-Dimensional (3D) CFD Predictions of Particle Distribution in Permeable Straight Tube

This section shows the results of calculations performed for a full 3D straight tube geometry using the NPHASE solver. Physical properties of the particle/liquid system under consideration are given in Table 2. Major geometrical and flow parameters are given in Table 3.

TABLE 2. Physical properties of particle-liquid system

Property	Liquid (water)	Particles (silica)
Density (ρ , kg/m ³)	1000.0	2200.0
Viscosity (μ , Pa-sec)	0.001	---
Characteristic Diameter (D , m)	---	10 ⁻⁶
Volumetric concentration (α_k)	0.9	0.1

TABLE 3. Geometry definitions and flow parameters used in the calculations

Case	Tube Radius (R_t , mm)	Curvature Radius (R_c , mm)	Average axial velocity (m/s)	Cross-flow velocity (v_w , m/s)	Re	De
<i>Straight Tube</i>	1.6	-	0.1	2×10^{-6}	320	0
<i>U-bend</i>	1.6	10	0.1	2×10^{-6}	320	128

The shear-induced diffusion force was calculated at every location using the model given by Eq.(17), where the shear-induced diffusion coefficient was taken as a function of particle volume fraction, according to Eq.(18). The local shear stress magnitude, $|\underline{\tau}|$, was calculated from the liquid shear stress tensor, $\underline{\tau}$, determined with respect to the liquid molecular viscosity, as

$$|\underline{\tau}| = \sqrt{\frac{1}{2}(\underline{\tau} \cdot \underline{\tau}^T)} = \sqrt{\frac{1}{2}\sum_i \sum_j \tau_{ij}^2} \quad (19)$$

The particle volume fraction profiles, predicted at near wall locations, are shown in Figure 2 for various axial locations. The minor increase in particle concentration in the main flow direction is due to the effect of the assumed uniform suction along the porous wall.

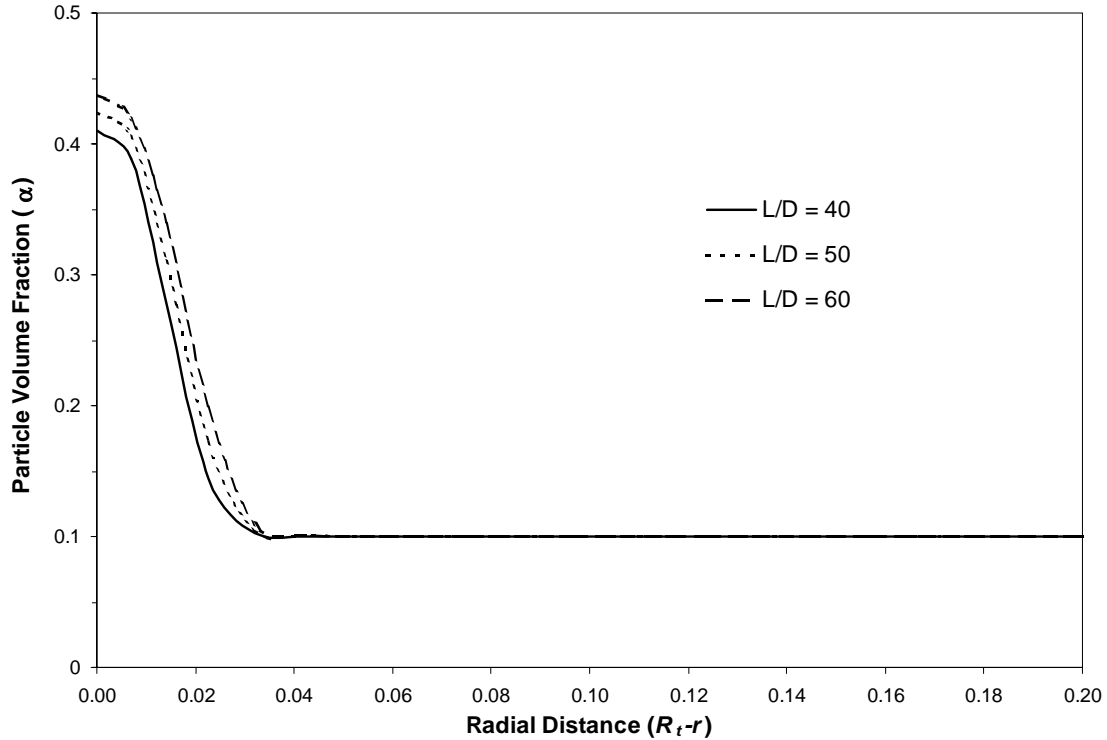


FIGURE 2. NPHASE predictions of the particle volume fraction distribution at various axial locations in the 3D straight tube given in Table 3.

The shear-induced diffusion coefficient was also calculated analytically, by balancing the drag and shear-induced diffusion force on a particle. For analytical calculations relative velocities predicted from the NPHASE solver at the $L/D = 60$ location of the straight tube, are used. Figure 3, shows the comparison for shear-induced dispersion coefficient, C_{SI} , between the CFD and the analytical calculation directly. A good agreement is predicted between both results. In the present calculations, the shear-induced diffusion coefficient varies dramatically with the particle volume fraction. Hence, a similar trend is observed for the shear-induced diffusion force. This effect can be seen in the particle volume fraction profiles.

4.2 Particle Distribution in U-bend

The model presented in Section 3 has been also used to make predictions for a full 3D *U-bend* geometry, as described in Table 3. Physical properties of the particle/liquid system are given in Table 2. A constant, radially outward, suction velocity, $\mathbf{v}_w = 2. \times 10^{-6} \text{ m/s}$, was assigned at the curved section of the U-bend. The shear-induced diffusion force was applied using Eq.(17).

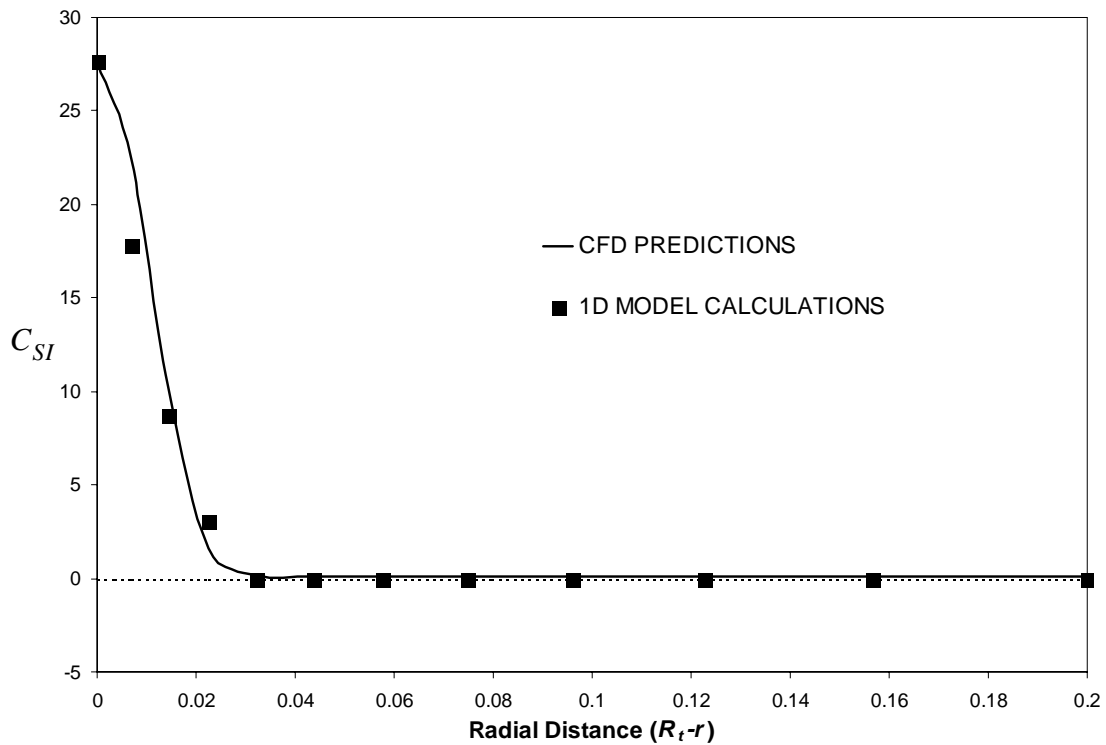


FIGURE 3. Radial distribution of the shear-induced dispersion coefficient across the straight tube given in Table 3; a comparison between the analytical calculation and the 3-D NPHASE predictions at the axial location of $L/D = 60$.

Figure 4 shows the azimuthal distribution of the near wall volume fraction at various axial locations in the U-bend. The volume fraction distribution in the U-bend case without suction, and for the straight tube case with suction, are also shown in Figure 4. The importance of secondary flow on particle distribution can be easily seen. It is observed that if no cross-flow was assigned to the curved wall, then a nearly uniform particle distribution was obtained along the curved U-bend tube. On the other hand, for the straight tube case with cross-flow, a uniform particle concentration has been obtained at all locations along the circumference of the wall; however, the volume fraction value in this case is much higher than the average bulk volume fraction. This effect is due to the cross-flow from the wall. Specifically, particles experience drag towards the wall due to the suction-induced liquid flow into, and across, the porous wall. At the wall, the drag force balances the shear-induced diffusion force, which results in an equilibrium concentration at the wall. This concentration is much higher than the average bulk concentration.

The volume fraction distribution for the straight tube shown in Figure 4 was obtained at the same axial location, equivalent to the 90° section (axially) of the U-bend. The most interesting result shown in Figure 4 is the particle distribution prediction for the U-bend with cross-flow. It is observed that the particle concentration at the wall is much lower than the concentration obtained for the straight tube case. Also, unlike for the straight tube, the particle concentration distribution is highly non-uniform along the circumference of the tube at various axial locations along the curved section of the U-bend. It is interesting to notice that the maximum particle concentration is predicted at the inner bend, and the minimum particle concentration is predicted at the outer bend. The reason for this is the variable vortex strength at different circumferential

locations. Plots of the magnitude of the corresponding near-wall vorticity can be found in Tiwari et al. [9]. It is evident that the highest strength is observed at the outer bend, which results in the lowest particle concentration at that location. The opposite is true for the inner bend.

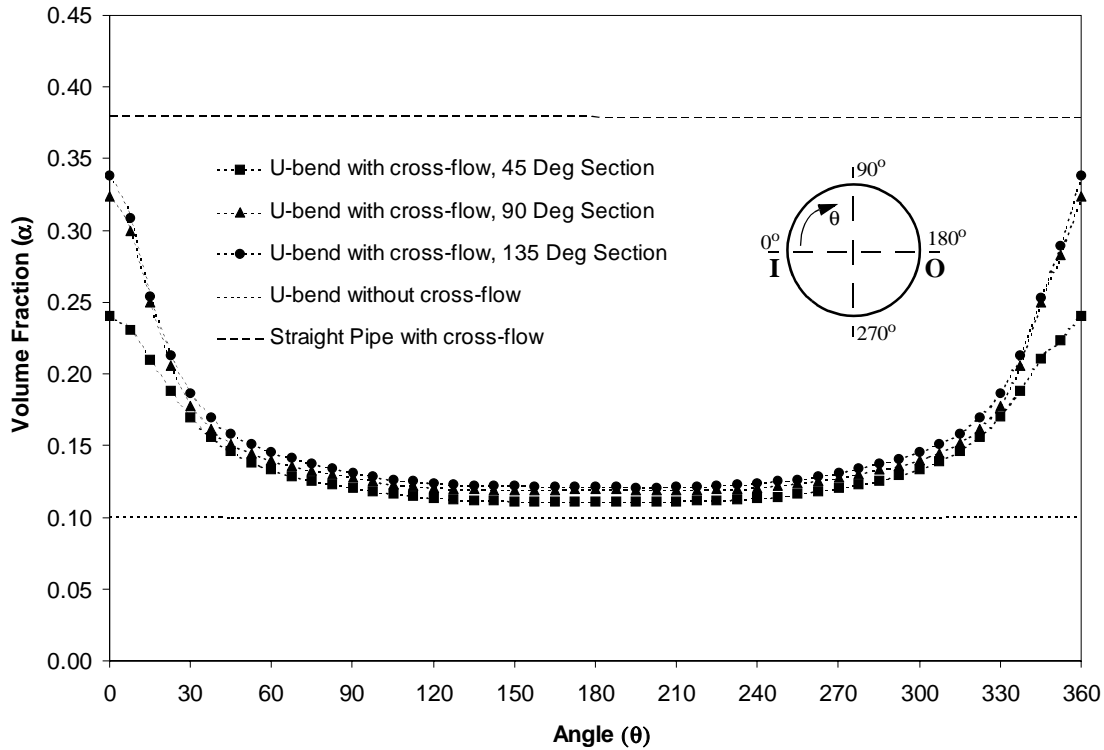


FIGURE 4. Circumferential particle concentration distribution at various axial locations in the U-bend case with cross-flow. The results are compared with those for a straight tube with cross-flow and for a U-bend case without cross flow.

Another important observation from Figure 4 is that the particle concentration in the U-bend for the case with cross-flow is always lower than for the straight tube case with cross-flow, and it is only slightly higher than that for the solid straight tube (i.e., without suction) for most circumferential distance around the tube wall. This effect is due to the presence of Dean vortices in the U-bend case, which helps to move particles away from the near-wall region.

5. Conclusions

Dilute liquid/particle two-phase flows in a permeable straight tubes and U-bends have been analyzed. The major aspects of the results are:

- A novel approach is proposed to model the shear-induced diffusion effect in 3-D curved membrane tubes that experience cross-flow at the porous wall
- The proposed shear-induced diffusion force model has been thoroughly tested and validated against analytical calculations, showing the consistency and numerical accuracy of the results

- Particle distributions in full 3D straight and U-bend permeable membrane tubes have been studied using a new model of the shear-induced diffusion force. It has been observed that Dean vortices play a significant role in particle distribution, and, in particular, dramatically mitigate particle buildup at the porous wall

References

- [1] Belfort, G., Davis, R. and Zydney, A., The behavior of suspensions and macromolecular solutions in crossflow microfiltration, A review for the North American Membrane Society's Annual Reviews and for the *J. Membrane Sci.*, **96**, 1-58 (1994).
- [2] Drew, D. A. and Passman, S. L., *Theory of multicomponent fluids*, Springer-Verlag New York Inc (1999).
- [3] Podowski, M.Z., Modeling of Two-Phase Flow and Heat Transfer; Remarks on Recent Advancements and Future Needs, *Proc. 3rd Int. Conf. on Transport Phenomena in Multiphase Systems*, Kielce, Poland (2002).
- [4] Blatt, W. F., David, A., Michaels, A. S. and Nelsen, L., Solute polarization and cake formation in membrane ultrafiltration: causes, consequences, and control techniques, In *Membrane Science and Technology* (Edited by L. Flinn), Plenum Press, New York, 47-97 (1970).
- [5] Bird, A. B., Stewart, W. E. and Lightfoot, E. N., *Transport Phenomena*, John Wiley & Sons Publishers (1994).
- [6] Eckstein, E. C., Bailey, P. G. and Shapiro, A. H., Self-diffusion of particles in shear flow of a suspension, *Jr. Fluid Mech.*, **79**, 191-208 (1977).
- [7] Leighton, D. and Acrivos, A., Measurement of shear-induced self diffusion in concentrated suspension of spheres, *Jr. Fluid Mech.*, **177**, 109-131 (1987).
- [8] Davis, R. H. and Leighton, D. T., Shear-induced transport of a particle layer along a porous wall, *Chem. Engg. Sci.*, **42** (2), 275-281 (1987).
- [9] Tiwari, P., Antal, S. P., Burgoyne, A., Belfort, G. and Podowski, M. Z., Multifield computational fluid dynamics model of particulate flow in curved circular tubes, *Theoret. Comput. Fluid Dynamics*, 2004 (in print).